Current Biology

Report

The cell cycle oscillator and spindle length set the speed of chromosome separation in *Drosophila* embryos

Highlights

- Chromosome separation speed decreases over the four *Drosophila* blastoderm cycles
- Anaphase spindle length reduction correlates with decreased chromosome speed
- Microtubule-depolymerizing and -sliding motors regulate chromosome velocity
- The cell cycle oscillator sets anaphase duration, impacting chromosome velocity

Authors

Yitong Xu, Anna Chao,
Melissa Rinaldin, Alison Kickuth,
Jan Brugués, Stefano Di Talia

Correspondence

stefano.ditalia@duke.edu

In brief

Xu et al. investigate how the speed of chromosome separation is regulated during the cleavage divisions of the *Drosophila* blastoderm. They find that spindle length and the cell cycle oscillator jointly control the velocity of chromosome movement in anaphase.

Xu et al., 2025, Current Biology *35*, 655–664
February 3, 2025 © 2024 Elsevier Inc. All rights are reserved, including those
for text and data mining, AI training, and similar technologies.
https://doi.org/10.1016/j.cub.2024.11.046

CellPress

Current Biology

CellPress

Report

The cell cycle oscillator and spindle length set the speed of chromosome separation in *Drosophila* embryos

Yitong Xu,[1,2] **Anna Chao**,[1,2] **Melissa Rinaldin**,[3,4,5] **Alison Kickuth**,[3,4,5] **Jan Brugués**,[3,4,5] **and Stefano Di Talia**[1,2,6,*]
[1]Department of Cell Biology, Duke University Medical Center, Durham, NC 27705, USA
[2]Duke Center for Quantitative Living Systems, Duke University Medical Center, Durham, NC 27710, USA
[3]Cluster of Excellence Physics of Life, TU Dresden, Dresden 01307, Germany
[4]Max Planck Institute of Molecular Cell Biology and Genetics, Dresden 01307, Germany
[5]Center of Systems Biology, Dresden 01307, Germany
[6]Lead contact
*Correspondence: stefano.ditalia@duke.edu
https://doi.org/10.1016/j.cub.2024.11.046

SUMMARY

Anaphase is tightly controlled spatiotemporally to ensure proper separation of chromosomes.[1–3] The mitotic spindle, the self-organized microtubule structure driving chromosome segregation, scales in size with the available cytoplasm.[4–7] Yet, the relationship between spindle size and chromosome movement remains poorly understood. Here, we address this relationship during the cleavage divisions of the *Drosophila* blastoderm. We show that the speed of chromosome separation gradually decreases during the four nuclear divisions of the blastoderm. This reduction in speed is accompanied by a similar reduction in spindle length, ensuring that these two quantities are tightly linked. Using a combination of genetic and quantitative imaging approaches, we find that two processes contribute to controlling the speed at which chromosomes move in anaphase: the activity of molecular motors important for microtubule depolymerization and sliding and the cell cycle oscillator. Specifically, we found that the levels of multiple kinesin-like proteins important for microtubule depolymerization, as well as kinesin-5, contribute to setting the speed of chromosome separation. This observation is further supported by the scaling of poleward flux rate with the length of the spindle. Perturbations of the cell cycle oscillator using heterozygous mutants of mitotic kinases and phosphatases revealed that the duration of anaphase increases during the blastoderm cycles and is the major regulator of chromosome velocity. Thus, our work suggests a link between the biochemical rate of mitotic exit and the forces exerted by the spindle. Collectively, we propose that the cell cycle oscillator and spindle length set the speed of chromosome separation in anaphase.

RESULTS

In *Drosophila* embryos, early development is characterized by rapid and synchronous syncytial nuclear divisions.[8,9] At the blastoderm stage, multiple divisions occur simultaneously on the surface of the embryo. These mitoses drive a reduction in the spacing among nuclei, which, in turn, results in smaller mitotic spindles. To elucidate the relationship between spindle size and chromosome separation, we used confocal live imaging to study anaphase in early fly embryos.

Using embryos maternally expressing histone tagged with GFP (His-GFP) and a microtubule fluorescent reporter (mCherry fused to the Tau microtubule-binding domain),[10] we imaged nuclear divisions and microtubule dynamics from cycle 10 to cycle 13 (Figures 1A and 1B). As nuclear cycles progressed, the number of nuclei at the surface of the embryo increased exponentially, while the spacing among nuclei proportionally reduced. As expected, mitotic spindles were proportionally smaller as the embryo approached later cycles (Figure 1A). We quantified the velocity of chromosome separation by measuring the speed at which the leading edges of segregating sister chromatids move apart from each other (Figures 1C and S1), estimated from images of the histone signal.[11] These measurements revealed that the speed at which chromosomes separate during anaphase exhibits a scaling relationship with spindle length (Figure 1H), estimated here as the maximum distance of chromosome separation (Figure S1D). This scaling ensures that chromosome separation has a similar duration (~70 s) in all nuclear cycles (Figures 1C and 1D). Moreover, the dynamics of the distance between sister chromosomes can be collapsed for all cycles when normalized by total distance that is covered in each cycle (Figure 1D), suggesting that the dynamics are essentially indistinguishable when rescaled for spindle length. Additionally, we found that both the movement of the chromosome toward the spindle pole (anaphase A) and the movement of spindle poles away from each other (anaphase B) demonstrated scaling with spindle length (Figures 1E–1G). Comparison of chromosome movements due to these two processes confirmed

© 2024 Elsevier Inc.
All rights are reserved, including those for text and data mining, AI training, and similar technologies.

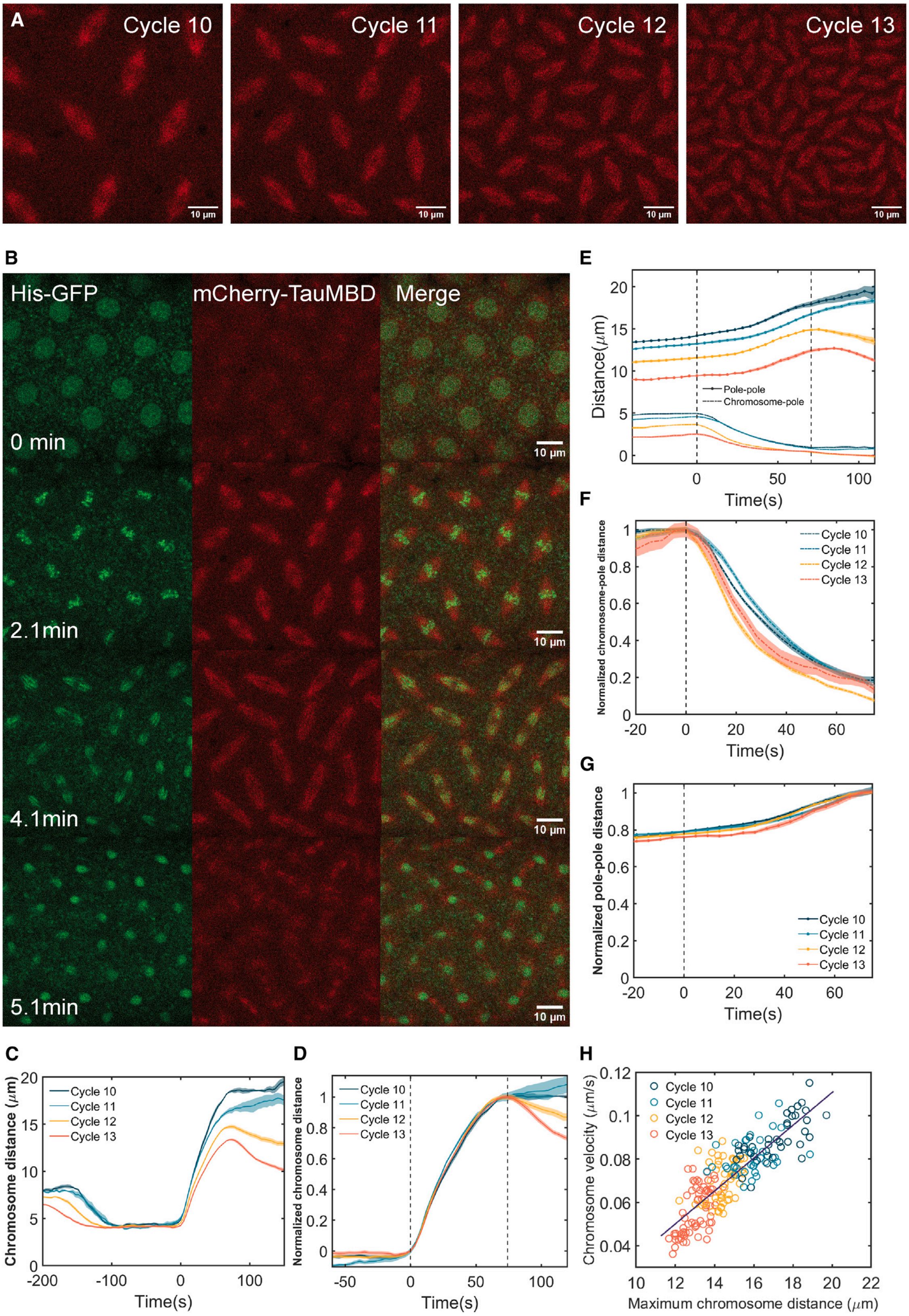

(legend on next page)

that chromosome separation is dominated by anaphase A (Figures 1F, 1G, and S1).[12,13] Collectively, these observations point to an interesting correlation between the speed of chromosome separation and the length of the mitotic spindle.

To elucidate this correlation, we first considered the potential role of microtubule dynamics. We conducted a series of experiments to quantify different parameters of spindle microtubule dynamics. First, we investigated microtubule density along the pole-to-pole axis during mitosis. As chromosomes separate and spindles elongate, the spatial distribution of microtubules remains largely unchanged, exhibiting no discernible correlation with chromosome (and kinetochore microtubules) position until the spindle disassembles (Figures 2A and 2B). Thus, in early anaphase, kinetochore microtubules likely represent a small fraction of spindle microtubules. The decrease in spindle length from cycle 10 to cycle 13 is accompanied by a decrease in microtubule density (Figures 2C and 2D). Secondly, we used embryos expressing the microtubule plus-end binding protein EB1-GFP[4,14–16] to quantify the rate of microtubule polymerization. Our analysis revealed that the polymerization velocity has a significant, although slight, dependency on spindle length, as it increases about 20% when spindle length doubles (Figures 2E and 2F). A similar positive correlation between spindle length and microtubule polymerization velocity has been observed in zebrafish, *C. elegans*, and sea urchin.[4,17] However, the extent of this correlation quantitatively changes in these organisms: a strong dependency is observed in sea urchin and *C. elegans*, while a small dependency is observed in zebrafish, similar to the one seen here. This observation argues that microtubule polymerization contributes partially to the modulation of spindle length in the *Drosophila* blastoderm. Finally, we employed femtosecond laser ablation to sever microtubules within the metaphase spindle to induce microtubule depolymerization.[18,19] A consistent rate of depolymerization of approximately 0.6 μm/s (35 μm/min) was observed, regardless of the specific cell cycle stage or spindle length, which demonstrated that the rate of depolymerization of unstable microtubules does not change during cycles 10–13 (Figures 2G and 2H). This observation and the fact that the measured value is consistent with values observed in other systems argue that this rate is set by the intrinsic properties of microtubule catastrophe dynamics. These observations on microtubule dynamics are similar to previous findings in zebrafish,[4] suggesting a conserved mechanism for the scaling of spindle size during *Drosophila* blastoderm divisions. However, they do not explain the relationship between spindle length and chromosome speed.

Poleward movement of chromosomes (anaphase A) is achieved by the shortening of kinetochore microtubules, while the separation of opposite spindle poles (anaphase B) is driven by microtubule sliding. Both processes involve forces generated on the microtubules by motor proteins. Thus, we turned our attention to the molecular motors involved in those processes and specifically motors that play a role in shortening kinetochore-associated microtubules, given the dominant contribution of anaphase A to chromosome separation. To this end, we first analyzed microtubule poleward flux, that is, the continuous movement of tubulin subunits toward the centrosome.[20–22] We note that for kinetochore-associated microtubules, poleward flux could be due to microtubule depolymerization at both the centrosome (minus end) and at the kinetochore (plus end), due to the activity of specific motors,[23–25] as well microtubule sliding. For interpolar microtubules, poleward flux could be due to either depolymerization at the centrosome or microtubule sliding. To estimate poleward flux in the fly embryos, we employed a transgenic line in which tubulin is tagged with a photo-convertible tandem dimer Eos fluorescent protein (tdEos) that can be converted from green to red upon UV illumination.[26] To describe poleward fluxes in anaphase, we monitored spindle morphology under the confocal microscope in live embryos.[27] As nuclei approached anaphase onset, we photo-converted a small region of microtubules near the mid-spindle and tracked it for 20–30 s during early anaphase (Figure 3A). The calculated poleward flux rates were comparable to the speed of chromosome movement at anaphase onset and similar to previously reported values.[22] The flux rate strongly correlated with spindle length, suggesting an involvement in setting the speed of chromosome movement in anaphase (Figure 3B).

To strengthen this point, we analyzed whether motors implicated in anaphase A and B movement, namely the kinesin-13 motors, Klp10A and Klp59C, the kinesin-8 Klp67A, and the kinesin-5 Klp61F, are rate-limiting for chromosome movements (Figure 3C). We used heterozygous mutants to lower their activity without abrogating it. We analyzed chromosome velocity and spindle length in these mutants and found that they retain a strong relationship between chromosome speed and spindle length. Notably, all heterozygous mutants display a significant reduction in the speed of chromosome separation for a given spindle length (Figures 3D–3F, quantifications are corrected for changes in spindle length due to loss of motor function). Similar effects were observed for motors acting primarily at the centrosome (Klp10A) and at the kinetochore (Klp67A and Klp59C),[24]

Figure 1. Chromosome velocity during anaphase scales with spindle length

(A) Mitotic spindles in the *Drosophila* embryo from syncytial cycle 10 to 13, labeled with mCherry-Tau microtubule-binding domain (mCherry-TauMBD).

(B) Chromosome and microtubule dynamics during mitosis in a His-GFP, mCherry-TauMDB embryo at cycle 11. From top to bottom: prophase, metaphase, anaphase, telophase.

(C) Distance between the leading edges of sister chromosomes during anaphase as a function of time in one embryo (cycle 10: $n = 4$, cycle 11: $n = 5$, cycle 12: $n = 16$, cycle 13: $n = 27$, mean ± SEM).

(D) Chromosome distance from (C) normalized by the distance traveled. Left dotted line: anaphase onset. Right dotted line: end of chromosome movement during anaphase, when chromosome distance reached its maximum or a plateau.

(E) Pole-to-pole distance and chromosome-to-pole distance in a His-RFP γ-tubulin-GFP embryo during anaphase (cycle 10: $n = 9$, cycles 11-13: $n = 6$ for each cycle, mean ± SEM).

(F and G) Both chromosome-to-pole distance and pole-to-pole distance in (E) could be rescaled across cycles.

(H) The average chromosome velocity during anaphase scales with the maximum chromosome distance, which serves as a proxy of spindle length ($N = 6$ embryos with His-GFP or His-RFP, $n = 190$ nuclear divisions). See also Figure S1 and Video S1.

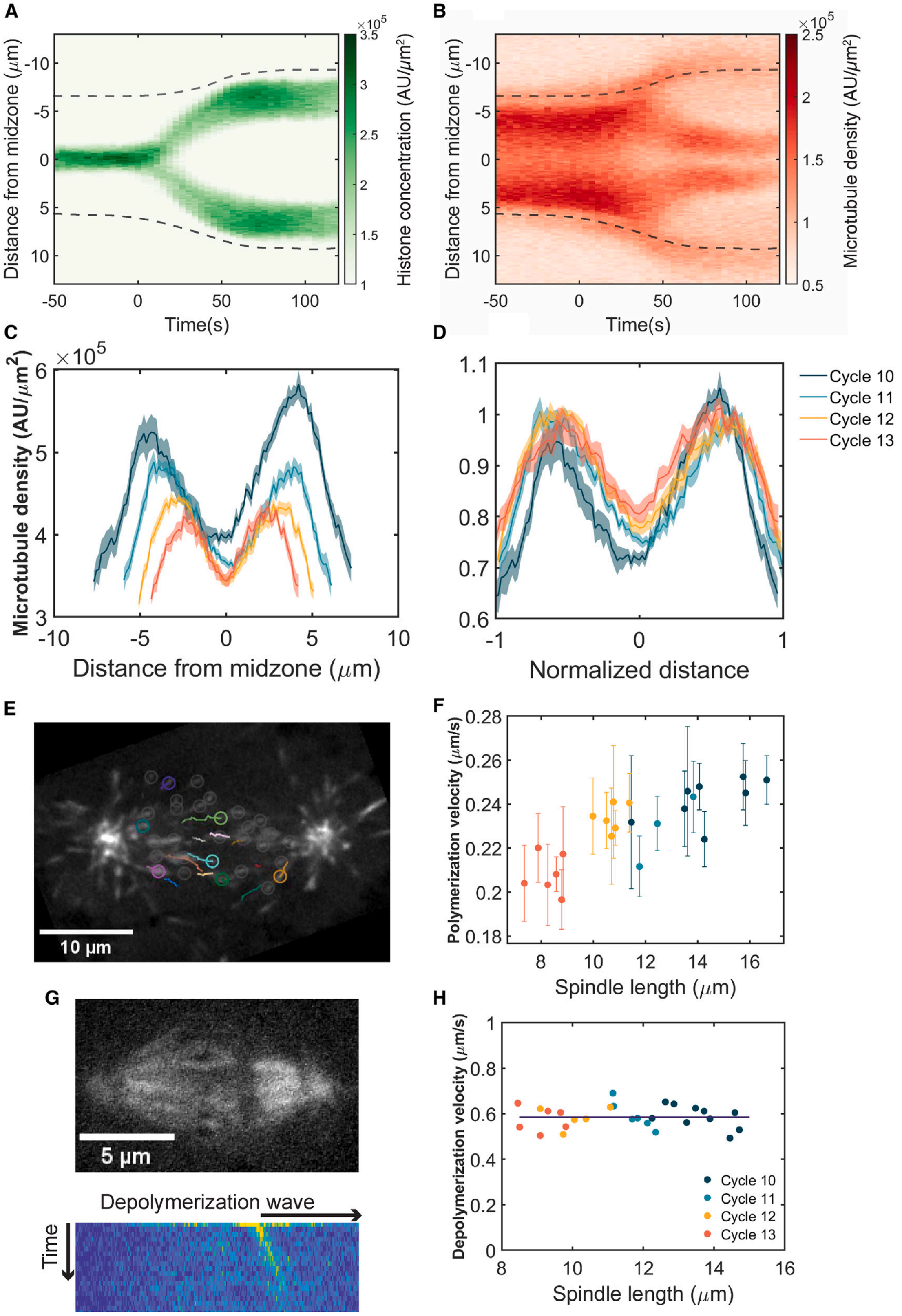

(legend on next page)

suggesting that both processes contribute comparably to chromosome movements (Figures 3D and 3F). Perturbing the level of Klp61F, the kinesin-5 motor driving microtubule sliding, also caused a slowdown of chromosome separation, as well as a small decrease in spindle length (Figures 3E and 3F), concordant with previous data.[28] In addition to anaphase B, kinesin-5 can influence anaphase A by coupling sliding interpolar microtubules to kinetochore fibers, as supported by severe inhibition of Klp61F function by antibody-induced dissociation of the motor from spindles.[28] Collectively, these results show that the scaling of chromosome movement with spindle length is the result of changes in the rate of microtubule polymerization, depolymerization, and sliding. These experiments implicate multiple motors in this process, suggesting that there might be a global mechanism controlling their activity in anaphase.

A natural candidate for such regulation is the cell cycle oscillator, as the activity of the motors must be controlled during the cell cycle. Specifically, we hypothesized that the rates of phosphorylation and dephosphorylation of mitotic targets involved in the function of the spindle influence the speed of chromosome separation. Changes in these rates likely set the timing of the completion of anaphase. We operationally defined anaphase duration as the time period from the initiation of chromosome segregation to nuclear envelope reformation (Figures 4A–4C), which we used as the hallmark event indicating completion of anaphase.[29,30] We used the intensity of nuclear-localized GFP to estimate the time when nuclear envelope integrity was reestablished. Imaging this probe together with histones showed that the reformation of the nuclear envelope starts after chromosome segregation is completed (Figure S2). We found that the duration of anaphase gets progressively longer from nuclear cycle 10 to 13 and, most importantly, that there is a strong correlation between anaphase duration and the speed of chromosome separation (Figure 4D).

To gain insight on this correlation, we investigated the relationship between chromosome speed and spindle length in embryos heterozygous for several regulators of the cell cycle (Figure 4E). We found that these mutations disrupt the scaling relationship. Embryos with one less copy of cyclin B (*1x cycB*) displayed slightly slower chromosome velocity, whereas embryos with two extra copies of cyclin B (*4x cycB*) exhibited a faster chromosome separation speed. We also observed a reduction of chromosome velocity in *polo* (Plk1) and *tws* (the B55 regulatory subunit of the PP2A phosphatase) heterozygous mutants. In *polo*/+ embryos, the nuclei migrating from the inner regions of the embryo reached the cortex at cycle 9,[31] which is one cycle earlier than in other genotypes, resulting in larger spindles at the onset of the blastoderm stage. Moreover, some *polo*/+ embryos failed to finish cycle 13 due to cell cycle defects and excessive crowding of the nuclei at the cortex. The *tws* heterozygous embryo (*twsP*/+) displayed normal spindle length despite slower chromosome speed than wild type. Finally, we found that *PP1-87B* and *PP1-96A* double heterozygous mutant embryos had slightly larger spindles and faster speeds than wild type (similar to *4x cycB*), suggesting that Cdk1 and PP1 have opposite impacts on chromosome separation. Collectively, these results revealed a major role for the components of the cell cycle oscillator in setting the speed of chromosome separation.

The cell cycle oscillator coordinates mitotic events in space and time (Figure 4C). In mitosis, Cdk1 activity represses cytoplasmic microtubule polymerization by affecting several microtubule-associated proteins and promotes spindle assembly and chromosome alignment.[32] Polo kinase also controls several aspects of spindle and centrosome behaviors.[33–35] The decrease of Cdk1 activity triggers the onset of anaphase and the migration of chromosomes toward the poles. As Cdk1 and Polo activities decrease in mitosis, mitotic substrates are dephosphorylated mainly by PP1/PP2A phosphatases.[36,37] The balance of mitotic kinases and phosphatases controls all events at mitotic exit, including chromosome decondensation and reformation of the nuclear envelope. Analysis of the duration of anaphase indicated that such duration is longer in the *cycB*/+, *polo*/+, and *twsP*/+ heterozygous embryos (Figure 4F). Conversely, *4x cycB* embryos and PP1 heterozygous embryos showed shorter anaphase durations than wild type. These findings support the hypothesis that the activity of cell cycle regulators sets the rate of completion of anaphase.

Given the observed changes in anaphase duration, we tested whether the speed of chromosome separation could be explained by these changes. Indeed, we found a strong correlation between chromosome velocity and anaphase rate, and that such correlation holds essentially for all the mutants analyzed, such that all the data can be collapsed on a single relationship (Figure 4F). This observation suggests that the rate of progression through anaphase is a strong predictor, and most likely the major regulator, of the speed of chromosome separation. Careful inspection of the data showed that in regions where the anaphase rate overlapped between wild-type and mutant embryos, the embryos with larger spindles tended to have slightly higher speeds. This observation suggested that there is a contribution to the speed of chromosome movement from processes

Figure 2. Microtubule dynamics contribute to spindle scaling in the *Drosophila* embryo

(A and B) Kymographs of chromosome separation (A) and spindle dynamics (B) in a cycle 11 embryo, labeled with His-GFP and mCherry-TauMBD. T = 0 indicates anaphase onset. Dashed lines indicate approximated centrosome positions.

(C) Line scans of microtubule density along the spindle long axis during metaphase in one embryo ($n = 5$ spindles for each cycle, mean ± SEM).

(D) Rescaled microtubule density from cycle 10 to 13.

(E) Microtubule plus-end tracking with EB1-GFP in a cycle 12 embryo.

(F) Microtubule polymerization velocity as a function of spindle length ($N = 7$, $n = 23$ spindles). Each data point represents the mean velocity ± SEM of all tracked comets in one spindle.

(G) Laser ablation of microtubules in a cycle 11 embryo, labeled with Jupiter-GFP. A wave of depolymerization was visualized after projecting the differential intensity onto the spindle long axis.

(H) Microtubule depolymerization velocity as a function of spindle length ($N = 27$). See also Videos S1, S2, and S3.

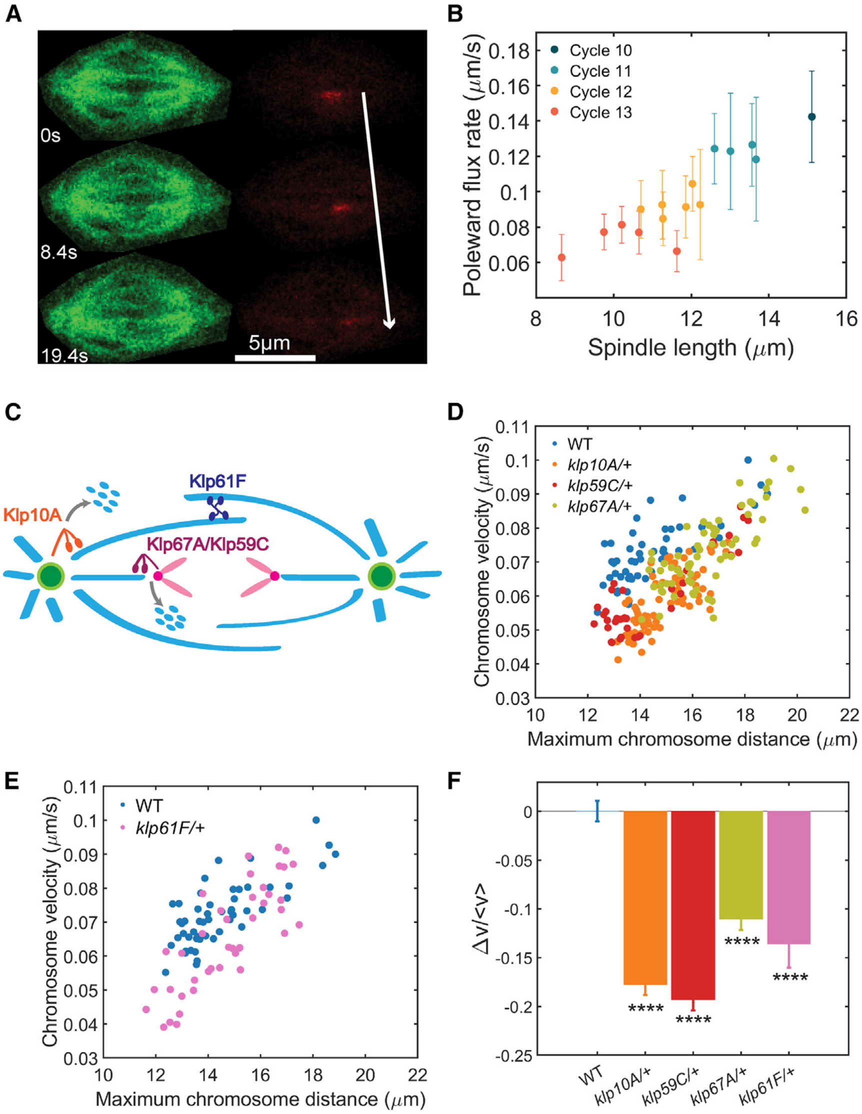

Figure 3. Microtubule-depolymerizing motors regulate chromosome velocity

(A) Photo-conversion of microtubules in the spindle using an α-tubulin-tdEos embryo.

(B) Poleward flux rate scales with spindle length (n = 16, mean ± 95% CI).

(C) Cartoon showing the activities of depolymerizing motors Klp10A, Klp59C, and Klp67A and microtubule-sliding motor Klp61F.

(D) Correlation between chromosome velocity and maximum chromosome distance in one wild-type (WT, n = 52), one Klp10A (n = 76), and one Klp67A (n = 65) heterozygous motor mutant.

(E) Correlation between chromosome velocity and maximum chromosome distance in one WT (n = 52) and two Klp61F (n = 40) heterozygous motor mutants.

(F) Average relative change in chromosome velocity between WT (N = 3, n = 91) and heterozygous motor mutants (*klp10A/+*: N = 3, n = 91; *klp59C/+*: N = 2, n = 53; *klp67A/+*: N = 3, n = 87; *klp61F/+*: N = 2, n = 40, mean ± SEM, **** $p < 0.0001$). See also Figure S3 and Video S4.

independent of anaphase duration. We speculated that this residual contribution arises from differences in spindle length and/or microtubule dynamics.[38] Thus, we used a simple linear model to test how much of the data can be captured by a combination of anaphase duration and spindle length. After centering and normalization of the two variables, we found that a linear combination of anaphase rate and spindle length can predict chromosome speed with high accuracy in all the mutants (R^2 = 0.84). This analysis suggests that anaphase rate accounts for 70% of the dependency of chromosome velocity, whereas residual contributions from spindle length (or a closely correlated variable) might explain the remaining 30% (Figure 4G). Collectively, these results argue that the speed of chromosome separation is set by a combination of biochemical cues from the cell cycle oscillator and additional mechanical cues from spindle length.

The previous analysis also suggested that PP2A-B55, rather than PP1, is the rate-limiting phosphatase for completion of anaphase. Thus, we set to establish a quantitative assay to determine whether PP2A-B55 activity changes during cycles 10–13 in a way that could explain the observed changes in the speed of chromosome separation. To this end, we analyzed the localization of Prc1/Feo to the spindle midzone (Figure S4A), as it was previously shown that in human cells such localization depends on the dephosphorylation of a Cdk1 site by PP2A-B55.[39,40] The site is relatively well conserved in *Drosophila* (Figure S4B), and we confirmed that PP2A-B55 is rate-limiting for Feo localization to the midzone by analyzing the rate of accumulation in wild-type vs. *twsP/+* mutants (Figure S4D). Remarkably, we found that the rate of accumulation of Feo to the midzone is a strong predictor of the speed of chromosome separation, supporting a role for PP2A-B55. Feo accumulates to the midzone during late anaphase (when chromosome separation is almost complete but prior to nuclear envelope reformation),[41] thus our assay infers PP2A-B55 activity late in anaphase (Figure 4C). We expect that this late activity correlates with the phosphatase activity throughout anaphase and thus conclude that the rate of activation of PP2A-B55 is a major regulator of chromosome velocity.

DISCUSSION

Anaphase is the culmination of mitosis when duplicated chromosomes segregate to opposite poles. Typically, anaphase accounts for a very short portion of the cell cycle.[42–44] The rapidity and precise spatial control needed for a successful anaphase could pose challenges for the accuracy of chromosome segregation. Here, we carefully characterized the

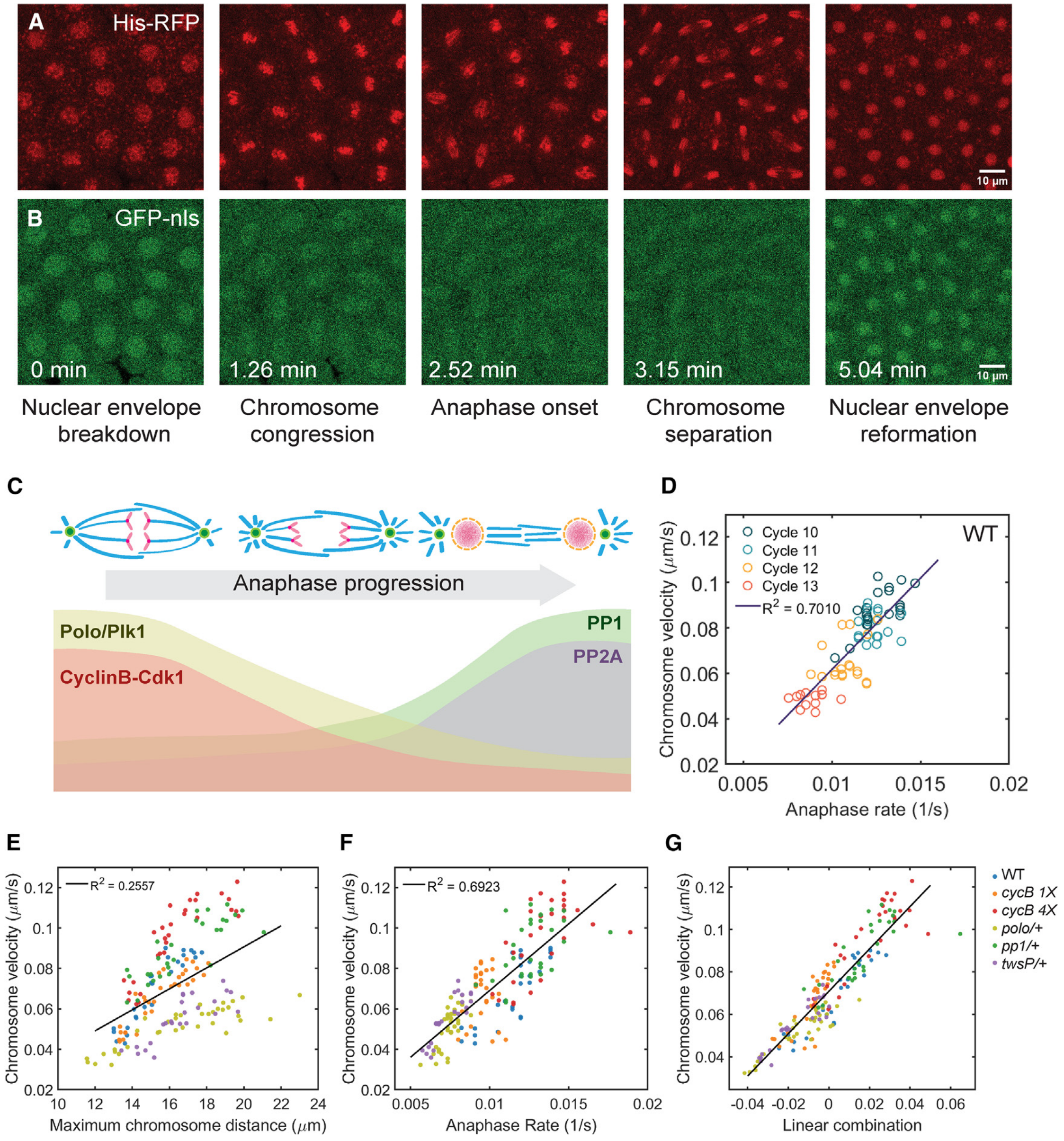

Figure 4. The cell cycle oscillator and spindle length together set the speed of chromosome movement in anaphase

(A and B) Dynamics of chromosome and nuclear localization signals (NLSs) in a cycle 11 embryo, from nuclear envelope breakdown to nuclear envelope reformation.

(C) Schematic of anaphase progression and the corresponding activity of mitotic kinases and phosphatases.

(D) Chromosome velocity scales with anaphase rate in WT embryos (*N* = 3, *n* = 71).

(E) Chromosome velocity as a function of maximum chromosome distance in individual heterozygous cell cycle mutant embryos (WT: *n* = 27; *cycB 1X*: *n* = 31; *cycB 4X*: *n* = 29; *polo*/+: *n* = 36; *pp1*/+: *n* = 29; *twsP*/+: *n* = 24).

(F) Chromosome velocity as a function of anaphase rate in heterozygous cell cycle mutants.

(G) Chromosome velocity scales with a linear combination of anaphase rate (70%) and spindle length (30%). See also Figures S2–S4.

movement of chromosomes during anaphase as *Drosophila* embryos proceed through the blastoderm cycles. We found that the speed of chromosome separation during these cycles is in large part controlled by the rate at which nuclei complete anaphase. Spindle length (microtubule dynamics) further contributes to this process, ensuring a tight relationship between chromosome separation and spindle length in *Drosophila* blastoderm embryos.

The mechanisms of chromosome segregation during anaphase vary across different biological systems. In *Drosophila* embryos and human cell lines, chromosome-to-pole movement (anaphase A) dominates the total chromosome movement. On the contrary, in *C. elegans* embryos, chromosome movement is almost solely achieved by pole-pole separation (anaphase B).[13] Our analysis of microtubule dynamics and our genetic manipulations of molecular motors argue the speed of chromosome separation is mainly set by the activity of microtubule-depolymerizing motors. Notably, all three microtubule-depolymerizing motors, Klp10A, Klp67A, and Klp59C, as well as kinesin-5 Klp61F, contribute to setting chromosome speed in anaphase. Two major drivers of anaphase A movement have been proposed: microtubule depolymerization at the centrosome and the kinetochore. It has been debated which of the two mechanisms contributed more. Our work argues that both processes contribute to a comparable extent to anaphase A.

Our results support a model in which the duration of anaphase is a major determinant of the speed of chromosome movement. This observation can be linked to the role of molecular motors by proposing that the cell cycle oscillator sets the activity of the motors and thus controls the speed of chromosome movement. This model is supported by previous experiments showing that phosphorylation by mitotic kinases can influence the activity of mitotic centromere-associated kinesin (MCAK), the major microtubule-depolymerizing kinesin in human cells.[45] Notably, we found that the rate of anaphase completion depends similarly on the activity of the mitotic kinases Polo and CycB-Cdk1 and the phosphatase PP2A. Genetic manipulations that decrease the activity of all three enzymes result in slower progression through anaphase. Our analysis also revealed that PP2A-B55, rather than PP1, is the rate-limiting phosphatase for timing nuclear envelope reformation (completion of anaphase), consistent with previous findings.[30] These observations suggest that the duration of anaphase depends on feedback mechanisms among Polo, Cdk1, and PP2A that drive both phosphorylation and dephosphorylation of mitotic targets. Understanding how these mechanisms operate to control anaphase will provide new insight on mitotic regulation.

Our experiments also show that cell cycle dynamics cannot fully explain the speed of chromosome separation and that other processes that correlate with or are controlled by spindle length must be involved. A possibility is that available molecular motors are titrated out by the increasing number of kinetochores and centrosomes. Consistent with this, using a Klp10A-GFP transgenic line, we observed a slight decrease in the Klp10A concentration at centrosomes from cycle 11 to cycle 13 (Figure S3A). Notably, the speed of chromosome separation in *klp10A*/+ and *klp67A*/+ embryos is reduced even though the duration of anaphase is essentially unaltered (Figure S3B), further suggesting that in addition to their control by the cell cycle, the levels and localization of these motors contribute to anaphase movements. Alternatively, the effects of spindle length on chromosome separation could arise from geometric or physical effects, for example via microtubule length-dependent processes or other mechanisms by which forces might scale with spindle length.[46] However, we cannot exclude that changes in microtubule dynamics affect both spindle length and chromosome velocity, and thus the effect of spindle length on chromosome separation is an indirect consequence of changes in microtubule dynamics.

Scaling of spindle size with available cytoplasm is ubiquitous, and it is believed that microtubule polymerization and nucleation set this scaling.[4,5] In this study, we revealed an association between spindle scaling and chromosome segregation. Understanding if this association is conserved in other systems, in particular in embryos undergoing reductive cleavage divisions, could reveal a general link between these processes. Furthermore, understanding if and how the scaling identified here is influenced by the syncytial and multi-nucleated nature of the cytoplasm will be important. In the future, developing an integrated model that combines the dynamics of phosphorylation levels, microtubule quantity and dynamics, and cell cycle progression will be essential to elucidate the mechanism of scaling of chromosome speed.

RESOURCE AVAILABILITY

Lead contact

Further information and requests for resources and reagents should be directed to and will be fulfilled by the lead contact, Stefano Di Talia (stefano.ditalia@duke.edu).

Materials availability

This study did not generate new fly lines or reagents.

Data and code availability

All the microscopy data reported in this paper will be shared by the lead contact upon request.

All original code has been deposited at Github at the following link and is publicly available as of the date of publication: https://github.com/Yitong-Xu/Scaling2024.

Any additional information required to reanalyze the data reported in this paper is available from the lead contact upon request.

ACKNOWLEDGMENTS

We thank the Bloomington Drosophila Stock Center, Sharyn Endow, David Glover, Michael Goldberg, and Pavel Tomancak for providing stocks. We thank Mary Elting, Sharyn Endow, Christine Field, Tim Mitchison, Antonio Pereira, and Jonathan Scholey for discussions. We thank members of the Di Talia lab for discussions. This work was supported by NIH R01-GM122936 and R35-GM153490. M.R. acknowledges funding from the Human Frontier of Science (Postdoctoral cross disciplinary fellowship LT000920/2020-C) and the European Molecular Biology Organization (Postdoctoral fellowship EMBO ALTF 597-2021). J.B., M.R., and A.K. acknowledge support from the Deutsche Forschungsgemeinschaft (DFG, German Research Foundation) under Germany's Excellence Strategy – EXC-2068 – 390729961 Cluster of Excellence Physics of Life of TU Dresden.

AUTHOR CONTRIBUTIONS

Conceptualization, Y.X. and S.D.T.; methodology, Y.X., J.B., and S.D.T.; software, Y.X.; formal analysis, Y.X. and S.D.T.; investigation, Y.X., A.C., M.R., and A.K.; writing, Y.X. and S.D.T.; visualization, Y.X. and S.D.T.; supervision, S.D.T. and J.B.; funding acquisition, S.D.T. and J.B.

DECLARATION OF INTERESTS

The authors declare no competing interests.

STAR★METHODS

Detailed methods are provided in the online version of this paper and include the following:

- KEY RESOURCES TABLE
- EXPERIMENTAL MODEL AND STUDY PARTICIPANT DETAILS
  - ○ Fly lines and husbandry
- METHOD DETAILS
  - ○ Embryo collection and processing
  - ○ Microscopy
  - ○ Microtubule plus end imaging
  - ○ Laser ablation experiments
  - ○ Photo-conversion experiments

- QUANTIFICATION AND STATISTICAL ANALYSIS
  - Chromosome segmentation and tracking
  - Quantification of chromosome distance and chromosome velocity
  - Quantification of Anaphase A and B movement
  - Comparison of maximum chromosome distance and anaphase spindle length
  - Quantification of microtubule density
  - Quantification of microtubule polymerization velocity
  - Quantification of microtubule depolymerization velocity
  - Quantification of poleward flux rate
  - Quantification of nuclear envelope reformation
  - Quantification of Feo accumulation rate

SUPPLEMENTAL INFORMATION

Supplemental information can be found online at https://doi.org/10.1016/j.cub.2024.11.046.

Received: June 14, 2024
Revised: October 23, 2024
Accepted: November 20, 2024
Published: January 9, 2025

REFERENCES

1. Asbury, C.L. (2017). Anaphase A: Disassembling Microtubules Move Chromosomes toward Spindle Poles. Biology *6*, 15. https://doi.org/10.3390/biology6010015.
2. Scholey, J.M., Civelekoglu-Scholey, G., and Brust-Mascher, I. (2016). Anaphase B. Biology (Basel) *5*, 51. https://doi.org/10.3390/biology5040051.
3. Afonso, O., Matos, I., Pereira, A.J., Aguiar, P., Lampson, M.A., and Maiato, H. (2014). Feedback control of chromosome separation by a midzone Aurora B gradient. Science *345*, 332–336. https://doi.org/10.1126/science.1251121.
4. Rieckhoff, E.M., Berndt, F., Elsner, M., Golfier, S., Decker, F., Ishihara, K., and Brugués, J. (2020). Spindle Scaling Is Governed by Cell Boundary Regulation of Microtubule Nucleation. Curr. Biol. *30*, 4973–4983.e10. https://doi.org/10.1016/j.cub.2020.10.093.
5. Wilbur, J.D., and Heald, R. (2013). Mitotic spindle scaling during Xenopus development by kif2a and importin α. eLife *2*, e00290. https://doi.org/10.7554/eLife.00290.
6. Hazel, J., Krutkramelis, K., Mooney, P., Tomschik, M., Gerow, K., Oakey, J., and Gatlin, J.C. (2013). Changes in cytoplasmic volume are sufficient to drive spindle scaling. Science *342*, 853–856. https://doi.org/10.1126/science.1243110.
7. Good, M.C., Vahey, M.D., Skandarajah, A., Fletcher, D.A., and Heald, R. (2013). Cytoplasmic Volume Modulates Spindle Size During Embryogenesis. Science *342*, 856–860. https://doi.org/10.1126/science.1243147.
8. Foe, V.E., and Alberts, B.M. (1983). Studies of nuclear and cytoplasmic behaviour during the five mitotic cycles that precede gastrulation in *Drosophila* embryogenesis. J. Cell Sci. *61*, 31–70.
9. Deneke, V.E., Melbinger, A., Vergassola, M., and Di Talia, S. (2016). Waves of Cdk1 Activity in S Phase Synchronize the Cell Cycle in *Drosophila* Embryos. Dev. Cell *38*, 399–412. https://doi.org/10.1016/j.devcel.2016.07.023.
10. Mooney, P., Sulerud, T., Pelletier, J.F., Dilsaver, M.R., Tomschik, M., Geisler, C., and Gatlin, J.C. (2017). Tau-based fluorescent protein fusions to visualize microtubules. Cytoskeleton (Hoboken) *74*, 221–232. https://doi.org/10.1002/cm.21368.
11. Berg, S., Kutra, D., Kroeger, T., Straehle, C.N., Kausler, B.X., Haubold, C., Schiegg, M., Ales, J., Beier, T., Rudy, M., et al. (2019). ilastik: interactive machine learning for (bio)image analysis. Nat. Methods *16*, 1226–1232. https://doi.org/10.1038/s41592-019-0582-9.
12. Brust-Mascher, I., and Scholey, J.M. (2002). Microtubule Flux and Sliding in Mitotic Spindles of *Drosophila* Embryos. Mol. Biol. Cell *13*, 3967–3975. https://doi.org/10.1091/mbc.02-05-0069.
13. Roostalu, J., Schiebel, E., and Khmelinskii, A. (2010). Cell cycle control of spindle elongation. Cell Cycle *9*, 1084–1090. https://doi.org/10.4161/cc.9.6.11017.
14. Liang, Z.-Y., Hallen, M.A., and Endow, S.A. (2009). Mature *Drosophila* Meiosis I Spindles Comprise Microtubules of Mixed Polarity. Curr. Biol. *19*, 163–168. https://doi.org/10.1016/j.cub.2008.12.017.
15. Schindelin, J., Arganda-Carreras, I., Frise, E., Kaynig, V., Longair, M., Pietzsch, T., Preibisch, S., Rueden, C., Saalfeld, S., Schmid, B., et al. (2012). Fiji: an open-source platform for biological-image analysis. Nat. Methods *9*, 676–682. https://doi.org/10.1038/nmeth.2019.
16. Ershov, D., Phan, M.-S., Pylvänäinen, J.W., Rigaud, S.U., Le Blanc, L., Charles-Orszag, A., Conway, J.R.W., Laine, R.F., Roy, N.H., Bonazzi, D., et al. (2022). TrackMate 7: integrating state-of-the-art segmentation algorithms into tracking pipelines. Nat. Methods *19*, 829–832. https://doi.org/10.1038/s41592-022-01507-1.
17. Lacroix, B., Letort, G., Pitayu, L., Sallé, J., Stefanutti, M., Maton, G., Ladouceur, A.-M., Canman, J.C., Maddox, P.S., Maddox, A.S., et al. (2018). Microtubule Dynamics Scale with Cell Size to Set Spindle Length and Assembly Timing. Dev. Cell *45*, 496–511.e6. https://doi.org/10.1016/j.devcel.2018.04.022.
18. Steinmeyer, J.D., Gilleland, C.L., Pardo-Martin, C., Angel, M., Rohde, C.B., Scott, M.A., and Yanik, M.F. (2010). Construction of a femtosecond laser microsurgery system. Nat. Protoc. *5*, 395–407. https://doi.org/10.1038/nprot.2010.4.
19. Decker, F., and Brugués, J. (2015). Chapter 5 - Dissecting microtubule structures by laser ablation. In Methods in Cell Biology, E.K. Paluch, ed. (Academic Press), pp. 61–75. https://doi.org/10.1016/bs.mcb.2014.11.004.
20. Desai, A., Maddox, P.S., Mitchison, T.J., and Salmon, E.D. (1998). Anaphase A Chromosome Movement and Poleward Spindle Microtubule Flux Occur At Similar Rates in Xenopus Extract Spindles. J. Cell Biol. *141*, 703–713. https://doi.org/10.1083/jcb.141.3.703.
21. Mitchison, T.J. (1989). Polewards microtubule flux in the mitotic spindle: evidence from photoactivation of fluorescence. J. Cell Biol. *109*, 637–652. https://doi.org/10.1083/jcb.109.2.637.
22. Maddox, P., Desai, A., Oegema, K., Mitchison, T.J., and Salmon, E.D. (2002). Poleward Microtubule Flux Is a Major Component of Spindle Dynamics and Anaphase A in Mitotic *Drosophila* Embryos. Curr. Biol. *12*, 1670–1674. https://doi.org/10.1016/S0960-9822(02)01183-1.
23. Gandhi, R., Bonaccorsi, S., Wentworth, D., Doxsey, S., Gatti, M., and Pereira, A. (2004). The *Drosophila* Kinesin-like Protein KLP67A Is Essential for Mitotic and Male Meiotic Spindle Assembly. Mol. Biol. Cell *15*, 121–131. https://doi.org/10.1091/mbc.e03-05-0342.
24. Sharp, D.J., Mennella, V., and Buster, D.W. (2005). KLP10A and KLP59C: The Dynamic Duo of Microtubule Depolymerization. Cell Cycle *4*, 1482–1485. https://doi.org/10.4161/cc.4.11.2116.
25. Matos, I., Pereira, A.J., Lince-Faria, M., Cameron, L.A., Salmon, E.D., and Maiato, H. (2009). Synchronizing chromosome segregation by flux-dependent force equalization at kinetochores. J. Cell Biol. *186*, 11–26. https://doi.org/10.1083/jcb.200904153.
26. Lu, W., Fox, P., Lakonishok, M., Davidson, M.W., and Gelfand, V.I. (2013). Initial Neurite Outgrowth in *Drosophila* Neurons Is Driven by Kinesin-Powered Microtubule Sliding. Curr. Biol. *23*, 1018–1023. https://doi.org/10.1016/j.cub.2013.04.050.
27. Girão, H., and Maiato, H. (2020). Measurement of Microtubule Half-Life and Poleward Flux in the Mitotic Spindle by Photoactivation of Fluorescent Tubulin (Springer), pp. 235–246. https://doi.org/10.1007/978-1-0716-0219-5_15.
28. Brust-Mascher, I., Sommi, P., Cheerambathur, D.K., and Scholey, J.M. (2009). Kinesin-5–dependent Poleward Flux and Spindle Length Control

in *Drosophila* Embryo Mitosis. Mol. Biol. Cell *20*, 1749–1762. https://doi.org/10.1091/mbc.e08-10-1033.

29. Haraguchi, T., and Hiraoka, Y. (2007). Breakdown and Reformation of the Nuclear Envelope. In Nuclear Dynamics: Molecular Biology and Visualization of the Nucleus, K. Nagata, and K. Takeyasu, eds. (Springer), pp. 89–106. https://doi.org/10.1007/978-4-431-30130-1_4.
30. Mehsen, H., Boudreau, V., Garrido, D., Bourouh, M., Larouche, M., Maddox, P.S., Swan, A., and Archambault, V. (2018). PP2A-B55 promotes nuclear envelope reformation after mitosis in *Drosophila*. J. Cell Biol. *217*, 4106–4123. https://doi.org/10.1083/jcb.201804018.
31. Hur, W., Mukherjee, A., Hayden, L., Lu, Z., Chao, A., Mitchell, N.P., Streichan, S.J., Vergassola, M., and Talia, S.D. (2023). Scale-independent topological interactions drive the first fate decision in the *Drosophila* embryo. Preprint at bioRxiv. https://doi.org/10.1101/2023.10.11.561879.
32. Serpico, A.F., Febbraro, F., Pisauro, C., and Grieco, D. (2022). Compartmentalized control of Cdk1 drives mitotic spindle assembly. Cell Rep. *38*, 110305. https://doi.org/10.1016/j.celrep.2022.110305.
33. Sunkel, C.E., and Glover, D.M. (1988). Polo, a mitotic mutant of *Drosophila* displaying abnormal spindle poles. J. Cell Sci. *89*, 25–38. https://doi.org/10.1242/jcs.89.1.25.
34. Glover, D.M. (2005). Polo kinase and progression through M phase in *Drosophila*: a perspective from the spindle poles. Oncogene *24*, 230–237. https://doi.org/10.1038/sj.onc.1208279.
35. Conde, C., Osswald, M., Barbosa, J., Moutinho-Santos, T., Pinheiro, D., Guimarães, S., Matos, I., Maiato, H., and Sunkel, C.E. (2013). *Drosophila* Polo regulates the spindle assembly checkpoint through Mps1-dependent BubR1 phosphorylation. EMBO J. *32*, 1761–1777. https://doi.org/10.1038/emboj.2013.109.
36. Nasa, I., and Kettenbach, A.N. (2018). Coordination of Protein Kinase and Phosphoprotein Phosphatase Activities in Mitosis. Front. Cell Dev. Biol. *6*, 30. https://doi.org/10.3389/fcell.2018.00030.
37. Kataria, M., and Yamano, H. (2019). Interplay between Phosphatases and the Anaphase-Promoting Complex/Cyclosome in Mitosis. Cells *8*, 814.
38. Pereira, A.J., Aguiar, P., Belsley, M., and Maiato, H. (2016). Inducible fluorescent speckle microscopy. J. Cell Biol. *212*, 245–255. https://doi.org/10.1083/jcb.201506128.
39. Cundell, M.J., Bastos, R.N., Zhang, T., Holder, J., Gruneberg, U., Novak, B., and Barr, F.A. (2013). The BEG (PP2A-B55/ENSA/Greatwall) pathway ensures cytokinesis follows chromosome separation. Mol. Cell *52*, 393–405. https://doi.org/10.1016/j.molcel.2013.09.005.
40. Cundell, M.J., Hutter, L.H., Nunes Bastos, R., Poser, E., Holder, J., Mohammed, S., Novak, B., and Barr, F.A. (2016). A PP2A-B55 recognition signal controls substrate dephosphorylation kinetics during mitotic exit. J. Cell Biol. *214*, 539–554. https://doi.org/10.1083/jcb.201606033.
41. Wang, H., Brust-Mascher, I., and Scholey, J.M. (2015). The microtubule cross-linker Feo controls the midzone stability, motor composition, and elongation of the anaphase B spindle in *Drosophila* embryos. Mol. Biol. Cell *26*, 1452–1462. https://doi.org/10.1091/mbc.e14-12-1631.
42. Brown, R. (1951). The Effects of Temperature on the Durations of the Different Stages of Cell Division in the Root-tip. J. Exp. Bot. *2*, 96–110. https://doi.org/10.1093/jxb/2.1.96.
43. Heath, I.B., and Rethoret, K. (1980). Temporal analysis of the nuclear cycle by serial section electron microscopy of the fungus, Saprolegnia ferax. Eur. J. Cell Biol. *21*, 208–213.
44. El-Alfy, M., and Leblond, C.P. (1987). Long duration of mitosis and consequences for the cell cycle concept, as seen in the isthmal cells of the mouse pyloric antrum. II. Duration of mitotic phases and cycle stages, and their relation to one another. Cell Tissue Kinet. *20*, 215–226. https://doi.org/10.1111/j.1365-2184.1987.tb01100.x.
45. McHugh, T., Zou, J., Volkov, V.A., Bertin, A., Talapatra, S.K., Rappsilber, J., Dogterom, M., and Welburn, J.P.I. (2019). The depolymerase activity of MCAK shows a graded response to Aurora B kinase phosphorylation through allosteric regulation. J. Cell Sci. *132*, jcs228353. https://doi.org/10.1242/jcs.228353.
46. Nicklas, R.B. (1965). Chromosome Velocity during Mitosis as a Function of Chromosome Size and Position. J. Cell Biol. *25*, 119–135. https://doi.org/10.1083/jcb.25.1.119.

STAR★METHODS

KEY RESOURCES TABLE

REAGENT or RESOURCE	SOURCE	IDENTIFIER
Chemicals, peptides, and recombinant proteins		
Halocarbon Oil 27	Sigma	Cat # 9002-83-9
Experimental models: Organisms/strains		
D. melanogaster: w; His2Av-EGFP; mCH-TMBD	S. Di Talia	N/A
D. melanogaster: w[1118]; P{w[+mC]=PTT-GA}Jupiter[G00147]	Bloomington	BDSC: 6836; FlyBase: FBst0006836
D. melanogaster: w[*]; P{w[+mC]=His2Av-mRFP1}II.2	Bloomington	BDSC: 23651; FlyBase: FBst0023651
D. melanogaster: w[1118]; P{w[+mC]=osk-GAL4::VP16}F/TM3, Sb[1]	Bloomington	BDSC: 44242; FlyBase: FBst0044242
D. melanogaster: w[*]; P{w[+mC]=UASp-alphaTub84B.tdEOS}7M	Bloomington	BDSC: 51314; FlyBase: FBst0051314
D. melanogaster: w[1118]; P{w[+mC]=ncd-Eb1.GFP}M1F3	Bloomington	BDSC: 57327; FlyBase: FBst0057327
D. melanogaster: w[*]; P{w[+mC]=Klp10A.GFP}M12M1	Bloomington	BDSC:57329; FlyBase: FBst0033963
D. melanogaster: w[1118]; P{w[+mC]=ncd-gammaTub37C.GFP}F13F3	Bloomington	BDSC:56831; FlyBase: FBst0056831
D. melanogaster: Klp10A[ThbA]/FM7iP{ActGFP}	S. Endow	N/A
D. melanogaster: Klp59C[ΔE38-V35]M17M1/SM5	S. Endow	N/A
D. melanogaster: w[*]; P{w[+mC]=Klp10A.GFP}M12M1	Bloomington	BDSC: 57329; FlyBase: FBst0057329
D. melanogaster: Klp61F[urc-1]/TM6B, Tb[1]	Bloomington	BDSC: 35508; FlyBase: FBst0035508
D. melanogaster: w[*]; P{w[+mC]=EP}Klp67A [322b24]/TM6B, Tb[1]	Bloomington	BDSC: 35507; FlyBase: FBst0035507
D. melanogaster: y[1] w[67c23]; P{w[+mC]=Ubi-GFP.nls}ID-2; P{Ubi-GFP.nls}ID-3	Bloomington	BDSC: 1691; FlyBase: FBst0001691
D. melanogaster: w;pCasPer-CycB/pCasPer-CycB;pCasPer-CycB/pCasPer-CycB	S. Di Talia	N/A
D. melanogaster: w[*]; CycB[2]/CyO, P{ry[+t7.2]=ftz-lacB}E3	Bloomington	BDSC: 6630; FlyBase: FBst0006630
D. melanogaster: y[1]; P{y[+mDint2] w[BR.E.BR]=SUPor-P}polo[KG03033] ry[506]/TM3, Sb[1] Ser[1]	Bloomington	BDSC: 13941; FlyBase: FBst0013941
D. melanogaster: w[*]; Pp1-87B[87Bg-3] e[1] Pp1alpha-96A[2]/TM6B, Tb[1]	Bloomington	BDSC: 23699; FlyBase: FBst0023699
D. melanogaster: w; Sp/CyO; twsP/TM6C, Tb, Sb	M. Goldberg	N/A
D. melanogaster: w[*]; P{w[+m]=Ubi-p63E-feo.GFP}3/TM3, Sb[1]*	Bloomington	BDSC: 59274; FlyBase: FBst0059274
Software and algorithms		
MATLAB R2023b	Mathworks	https://www.mathworks.com/
ilastik	Berg et al.[11]	https://www.ilastik.org/
FIJI	Schindelin et al.[15]	https://imagej.net/software/fiji/
TrackMate	Ershov et al.[16]	https://imagej.net/plugins/trackmate/

EXPERIMENTAL MODEL AND STUDY PARTICIPANT DETAILS

Fly lines and husbandry

Klp10A P mutant flies were raised at room temperature (~21°C) on glucose food (Archon, Cat #D210). All other flies were raised at room temperature on standard molasses food (Archon, Cat #B20101).

METHOD DETAILS

Embryo collection and processing

Before imaging, adult flies with genotypes of interest were housed in a cage covering an apple juice plate at 25°C, supplemented with yeast paste. Embryos were collected over 2 hours on a fresh plate, dechorionated with 50% bleach for 1 minute, and mounted in Halocarbon oil 27 on a gas-permeable membrane with coverslips.

Microscopy

Embryos were imaged on a Leica SP8 laser scanning confocal microscope equipped with a Leica 20x oil-immersion objective 0.75NA (HC PL APO CS2 20x/0.75 IMM) unless otherwise noted.

Microtubule plus end imaging

Embryos were imaged with a spinning disk confocal microscope (IX83 Olympus microscope with CSU-X1 Yokogawa disk) connected with two iXon DU-897 back-illuminated EMCCD camera (Andor). Experiments were acquired using an Olympus 100x silicon oil objective1.35 NA and imaged at 1-2 frames per second.

Laser ablation experiments

With the Jupiter-GFP line, metaphase spindles were imaged using a spinning disk confocal microscope (Nikon Ti Eclipse, Yokogawa CSU-X1) equipped with an EMCCD camera (iXon DU-888 or DU-897, Andor) and a 100x oil-immersion objective. Images were acquired with the Andor iQ software. Laser ablation was performed according to Rieckhoff et al. on a custom-built femtosecond laser microsurgery system. Briefly, line cuts parallel to the spindle equator were induced by moving the sample with a high-precision piezo stage (PInano) relative to the stationary cutting laser. The ablation was controlled by a custom-written software managing the piezo-stage and a mechanical shutter in the optical path. Each embryo was cut only once and imaged at intervals of 200-300ms/frame.

Photo-conversion experiments

Photo-conversion experiments were performed on the Leica SP8 microscope with the FRAP Module in the Leica Application Suite X (LAS X). Experiments were acquired using a Leica 63x oil objective 1.40 NA (HC PL APO CS2 63x/1.40 OIL). Spindle microtubules were excited with 0.1% 405nm laser for 1 millisecond to induce photo-conversion from GFP to RFP.

QUANTIFICATION AND STATISTICAL ANALYSIS

Chromosome segmentation and tracking

Movies of the histone channel were loaded in ilastik for chromosome segmentation using the pixel classification workflow. Pixels were manually annotated as either chromosome or cytosol to train the classifier. Training was considered complete when the live output aligned with visual judgement. A prediction map for chromosome segmentation was generated. The raw movie and prediction map were reloaded into ilastik for the tracking or manual tracking workflow, with the division events manually labeled. For automatic tracking, the correctness of the tracking was manually verified before further quantification. Either the maximum number of trackable nuclear division events in frame or at least five divisions were recorded for each cycle.

Quantification of chromosome distance and chromosome velocity

For segmented chromosome undergoing mitosis, a bounding box was drawn surrounding a single nucleus or sister chromosomes. The length of the bounding box along the division axis was quantified as chromosome distance in real-time. Anaphase onset was determined as the first frame when chromosome distance started to increase after metaphase. The total chromosome movement during anaphase was quantified from anaphase onset till the chromosome distance plateaued (e.g. in cycles 10 and 11) or reached maximum before recoil (e.g. in cycles 12 and 13). Average chromosome velocity was calculated as total chromosome movement divided by the duration of the movement. To compare the velocity among genotypes controlling for spindle length, data points were divided into 4 bins based on spindle lengths (ranging from 12 μm to 20 μm). The average chromosome velocity of the wild-type in these bins was quantified as a refence velocity $<v_{WT}>$. For each bin, the relative change in velocity was quantified as $(v_{mutant}-<v_{WT}>)/<v_{WT}>$. Relative changes in all bins were summarized for each genotype.

Quantification of Anaphase A and B movement

Using the TrackMate plugin in FIJI, centrosomes marked with γTubulin were detected with the LoG detector and tracked with the LAP tracker, allowing for splitting. Centrosome tracks were manually curated and matched with the corresponding chromosome tracks. Anaphase B movement was quantified by measuring the separation of two centrosomes at opposite spindle poles. Anaphase A movement was calculated by subtracting Anaphase B movement from the total chromosome movement.

Comparison of maximum chromosome distance and anaphase spindle length

Maximum chromosome distance was measured using the His-GFP channel, while spindle length was measured using the mCherry-TauMBD channel. For each genotype, measurements were taken from one embryo from cycle 10 to 13. In each cycle, the anaphase spindle length and maximum chromosome distance were quantified across 3 nuclear divisions. Anaphase spindle length was manually measured as the centrosome-to-centrosome when the chromosomes were clearly separated, and the spindle exhibited an elongated shape characteristic of anaphase, but before the formation of the dense midzone region typical of telophase. The maximum chromosome distance for each division was also manually recorded. For each nuclear division, the ratio of maximum chromosome distance to anaphase spindle length was calculated. This ratio was then averaged for each genotype.

Quantification of microtubule density

For spindles at metaphase, a line of defined thickness (2μm) along the spindle long axis was used to measure fluorescence intensity and calculate the density profile.

Quantification of microtubule polymerization velocity

EB1 comets in the spindle region were tracked with the TrackMate plugin in the FIJI software, applying the LoG detector and simple LAP tracker. Tracks were filtered by duration (∼3-15s) and linearity (> ∼0.9) and then manually screened. The speeds of all correctly tracked comets within each spindle were averaged to represent the microtubule polymerization velocity for that spindle.

Quantification of microtubule depolymerization velocity

The amount of depolymerized microtubule during a time interval was calculated by subtracting raw images with a time difference of 0.4∼0.6s from each other and integrating these differential intensities perpendicular to the spindle long axis. Depending on the position of the cut, the integrated differential intensities along the spindle long axis showed one or two well-defined peaks. The peaks moved toward the nearest pole following ablation. The more prominent peak was fit to a Gaussian function to quantify the position of the maximum. The position of the maxima over time was fit to a line to determine the microtubule depolymerization velocity.

Quantification of poleward flux rate

To analyze the poleward flux, for images in the photo-converted channel, we computed the average fluorescence intensity along the spindle length and evaluated the points where this quantity crosses a value close to half-max, estimated as half of the 95 percentile of fluorescence intensity values. These points defined the ends of the photo-converted region. For instances when the spindles remain a constant length and where microtubules on both sides of the mid-spindle were properly labeled, the speed of poleward flux was estimated as half of the speed at which the two ends moved apart. For instances where microtubules were labeled only on one side of the spindle, we computed the speed as the distance between the photo-converted end and the closest centrosome. The positions of centrosomes were estimated by computing the initial and final positions where intensity in the green (non-converted) channel crossed a value close to half-max (half of the 95 percentile of fluorescence intensity values).

Quantification of nuclear envelope reformation

The Histone-RFP channel in the time-lapse movie was used to segment nuclei and track nuclear division with ilastik. The nuclear concentration of GFP-NLS signal, together with chromosome distance, was plotted as a function of time. The onset of nuclear envelope reformation was inferred from the time point when the GFP-NLS concentration began to increase after chromosome separation.

Quantification of Feo accumulation rate

A rectangle was defined at the centroid of segmented chromosome(s) (15μm along the spindle long axis * 2μm perpendicular to the spindle long axis). The average Feo intensity in the rectangular region was quantified and plotted against time. The Feo accumulation rate was determined by calculating the slope of the linear increase in the logarithm of average Feo intensity over time.